Journal of
Materials Chemistry C

Materials for optical, magnetic and electronic devices

Accepted Manuscript

This article can be cited before page numbers have been issued, to do this please use: J. C. Germino, R. Araujo Mendes, L. T. A. Duarte, F. S. Rodembusch, R. L. A. Haiduke and L. Pereira, *J. Mater. Chem. C*, 2026, DOI: 10.1039/D6TC00213G.

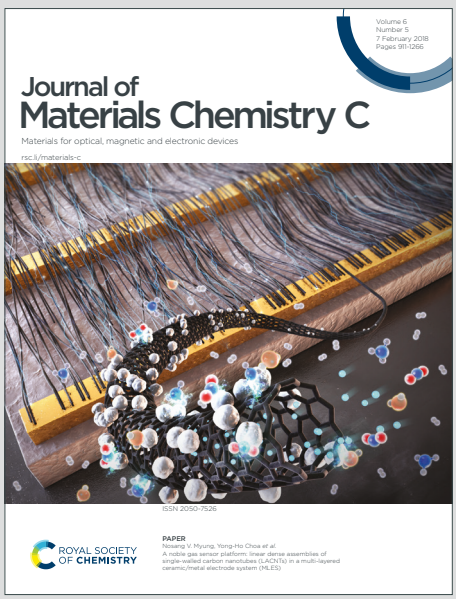

ROYAL SOCIETY OF CHEMISTRY

rsc.li/materials-c

View Article Online
DOI: 10.1039/D6TC00213G

ARTICLE

Charge Carrier Transport and Trap Levels on Solution-Processed Zn(II) Schiff Bases OLEDs

Received 00th January 20xx,
Accepted 00th January 20xx

DOI: 10.1039/x0xx00000x

José Carlos Germino,[a*] Rodrigo Araujo Mendes,[b] Luís Gustavo Teixeira Alves Duarte,[c] Fabiano Severo Rodembusch,[d] Roberto L. A. Haiduke,[e] and Luiz Pereira[a*]

Organic light-emitting diodes (OLEDs) are a leading display technology, yet achieving high efficiency in first-class fluorescent OLEDs remains a challenge due to limited internal quantum efficiency (IQE). In this study, we report a comprehensive investigation of Zn(II) Schiff base coordination compounds as first-class fluorescent emitters embedded in solution-processed active layers based on poly(9,9′-dioctylfluorene) (PFO). To enhance charge-carrier balance and device performance, two strategies were employed: (i) introduction of a TPBi electron-transport layer (ETL) and (ii) incorporation of the n-type material OXD-7 into the PFO matrix, forming an exciplex host. Devices fabricated from both room-temperature and hot solutions were characterized. Electroluminescence spectra revealed near-white emission due to efficient energy transfer between the host and guest materials. Charge-transport analysis using space-charge limited current (SCLC) models revealed that hot processing increases trap densities (NT), while OXD-7 incorporation reduces NT under cold processing. Among the emitters, Zn(BTS) and Zn(sal-3,4-ben) showed the highest device efficiencies in PFO and PFO:OXD-7 matrices, respectively, achieving current efficiencies up to 10.48 cd A^{-1} and EQEs exceeding 6%. The results demonstrate improved charge balance and reduced roll-off behavior, linking electrical and optical properties through quantitative trap-state analysis and electronic mobility estimations. This study provides a route to high-performance, cost-effective near-white OLEDs based on Earth-abundant Zn(II) coordination complexes.

Introduction

Since early studies by Tang and Van Slyke,[1] organic light-emitting diodes (OLEDs) have attracted the attention of physicists, chemists, materials scientists, and engineers due to their wide range of possibilities for fundamental innovations (charge–carrier transport and recombination mechanisms)[2], easy colour and efficiency tunability via slight chemical modifications[3], flexible[4] and biodegradable[5] substrates, and processing possibilities from classical thermal evaporation techniques to solution-processable protocols[6] (spin-coating[7], blade-coating[8], inkjet[9], slot-die[10], among others). Combining these characteristics, OLEDs have become efficient and competitive durable devices, ranging from cell phone display screens (RGB diodes)[11] to ambient lighting (white OLEDs, WOLEDs)[12] applications. Despite this, the understanding of some fundamental issues was left out due to an efficiency race. This fact has changed with the establishment of OLED technology.

Classical emissive materials for OLED applications must be separated into first- and second-class fluorescent systems and room-temperature phosphorescent molecular systems[13,14]. The main difference between these two photoluminescent compounds is directly related to the fermionic particle statistic: one-quarter of the injected charge carriers present singlet symmetry, whereas three-quarters are triplets. Thus, the internal quantum efficiency (IQE) of OLEDs assembled with first-class fluorescent emitters as an active layer is limited to 25% owing to this particular feature. Moreover, room-temperature phosphorescent materials can present an IQE of approximately 100% if the intersystem crossing (ISC) and photoluminescence quantum yield (PLQY) of the material are 100%[15], due to the strong spin-orbit coupling between the coordinated transition metal ion and the organic coordination sphere.[14] Nonetheless, owing to external outcoupling by subsequent layers (PEDOT:PSS, ITO, and glass, commonly), the maximum expected external quantum efficiency (EQE) of a first-class emitter for the OLED active layer is approximately 5%[16]. Compared with fluorescent materials, phosphorescent materials can produce highly efficient devices. However, to achieve room-temperature phosphorescence, organic molecules (ligands) must be bound to expensive and rare transition metal cations, such as iridium(III)[17], gold(I/III)[18], rhenium(I)[19], osmium(II)[20], and platinum(II)[21], among others[22], which are the major drawbacks of these kinds of materials[23]. These heavy metals confer to the molecule an efficient ISC process in the excited state, from the first singlet to the first

[a]*i3N – Institute of Nanostructures, Nanomodeling and Nanofabrication, Department of Physics, University of Aveiro, Aveiro 3810-193, Portugal*
[b]*Quantum Theory Project, University of Florida, Gainesville, Florida 32611, USA*
[c]*Chemistry Institute, University of Campinas, Campinas – SP, Brazil*
dChemistry Institute, Federal University of Rio Grande do Sul, Porto Alegre – RS, Brazil
[e]*São Carlos Institute of Chemistry, University of São Paulo, Av. Trabalhador São-Carlense, 400, CP 780, 13560-970 São Carlos, SP, Brazil*
*Corresponding authors: J.C.G (germino@ua.pt) and L.P (luiz@ua.pt).
†Electronic Supplementary Information (ESI) available. See DOI: 10.1039/x0xx00000x

View Article Online
DOI: 10.1039/D5TC00812G

triplet ($S_1 \rightarrow T_1$), which is emitted via a spin-forbidden pathway ($T_1 \rightarrow S_0$).

In addition to purely organic donor-acceptor systems, thermally activated delayed fluorescence (TADF) has also been demonstrated high-performance electroluminescence.[24] In special, metal-containing TADF coordination, including Cu(I)[25–27] and rationally engineered Pt(II)[28,29] compounds, where small singlet-triplet energy gaps enable efficient reverse ISC (rISC) and near-unity internal quantum efficiencies. Recent studies have shown that such metal-based TADF emitters can deliver high device efficiencies, in some cases approaching or exceeding the conventional outcoupling limit when combined with optimized optical architectures.[30] While these systems represent a significant advance beyond conventional phosphorescent emitters, they often require precise excited-state engineering and, in the case of noble-metal systems, relatively scarce elements.

On the other hand, fluorescent emitters are mainly composed of pure organic molecules or organic ligands coordinated to low-cost closed-shell cations, such as Al(III)[31] and Zn(II)[32]. The only role of these cations is to improve the molecular rigidity and stability of the system[33], which improves its nonlinear electronic absorption capacity, radiative recombination pathways, and charge–carrier transport characteristics. In particular, Zn(II) fluorescent materials have been intensively studied because Zn(II) is a nontoxic, Earth-abundant, and electronic-structured "inert" cation[34], enabling the use of its molecular organic coordinated materials for bioimaging confocal and epifluorescence microscopy, as well as emissive-guests[35] and charge-transport materials[36] for optoelectronic purposes.

In our previous reports involving the electroluminescence of asymmetric Zn(II) Schiff base coordination compounds (a type of first-class green–yellowish emitter), we were able to correlate the total charge–carrier mobility (μ) and photoluminescence quantum yields (PLQYs) of Zn(salophen) and Zn(sal-3,4-ben) with the device current efficiency of poly-N(vinyl carbazole) (PVK)-based diodes, which suggests the intrinsic role of the benzoyl moiety in the salophen electronic structure and its OLED figures of merit[37]. Second, we changed the PVK host to poly(9,9'-dioctylfluorene) (PFO), a p-type semiconducting polymer that simultaneously has a higher μ and PLQY and better spectral overlap with the Zn(II) compound absorption spectra than PVK. Later, we performed on another modification of the Zn(salophen) structure with the addition of the benzothiazole moiety, resulting in the Zn(BTS) complex[38]. This was a very successful strategy for improving the OLED figures of merit. In addition, we were able to achieve near-white OLEDs by combining the blue and green-yellow electroluminescence of PFO and the Zn(II) complexes, with high brightness values (3000 cd m^{-2}), which are 22 times greater than those of PVK-based diodes. In addition, a considerable improvement in the apparent charge–carrier mobility was observed when PFO was used at the counterpoint of PVK. We observed that the insertion of the benzoyl and the benzothiazole moieties in the salophen structures did not significantly change the optical properties in terms of absorption and emission energies; however, Density Functional Theory (DFT) calculations and time-resolved emission decays have shown that those chemical modifications completely change the frontier orbitals and their charge carrier dynamics in the excited state, creating a quasi-charge transfer state. These features were able to enhance the devices' charge–carrier mobility in comparison to PFO (neat) and PFO:Zn(salophen) OLEDs, according to the Mott–Gurney space–charge law in the trap–charge limited–current (TCLC) domain ($J \alpha V^n$; $n > 2$). Nevertheless, the best OLED obtained in this work had inferior figures of merit in terms of current efficiency ($\eta_C = 0.52$ cd A^{-1}) and low roll-off, despite being the best result for Zn(II) Schiff base OLEDs.

With the development of OLED science and technology, new strategies have been adopted by materials and device developers for breaking diodes' theoretical limits[39]: i) aggregated-induced emission; ii) delayed fluorescence materials (third class); and iii) molecular exciplex and energy transfer-based hosts (fourth class). In the last case, a long-lived spin/symmetry forbidden excited state can be formed due to the presence of a charge-transfer state between the HOMO and LUMO levels of the acceptor and donor materials, respectively. Owing to these characteristics, the exciplex state can be quickly transferred to the emissive material inside the host matrix[40]. Nevertheless, there is still room for improvement on the OLED figures of the merits of first-, second-, and third-class emissive molecules.

Taking into account these considerations, herein, we present two strategies to enhance the optical-electronic properties of PFO-based solution-processable layers containing Zn(salophen), Zn(sal-3,4-ben), and Zn(BTS) (Figure 1a) first-class emitter coordination compounds: 1) the addition of an electron transport layer (2,2',2''-(1,3,5-benzyl)-tris(1-phenyl-1-H-benzimidazole) – TPBi) between the active layer and the cathode (LiF|Al) and 2) the addition of the 1,3-bis[2-(4-tert-butylphenyl)-1,3,4-oxadiazo-5-yl]benzene (OXD-7 – electron transport material) in the PFO for assembling a fourth-class active matrix (PFO:OXD-7 – 3:2) as a host for Zn(II) Schiff base complexes, in addition to the use of TPBi as ETL. As a general trend, the insertion of the TPBi, a well-known electron transport and hole-blocking material[41,42], in the PFO-based diodes drastically enhances their figures of merit compared with the previous results, maintaining PFO:Zn(BTS) as the most efficient active layer, increasing approximately 20 times its figures of merit. On the other hand, the PFO:OXD-7 host promotes Zn(sal-3,4-ben) as the most efficient Zn(II) coordination compound in contrast to the Zn(BTS) molecule. For Zn(sal-3,4-ben), the addition of OXD-7, an electron transport material able to form an exciplex host[43] with PFO, increases the devices' figure of merit 17 and 3 times in comparison to our previous work and its PFO device, respectively. In fact, the addition of the OXD-7 ETM into the PFO semiconductive polymer decreases the OLED maximum brightness; however, the number of injected charge carriers is lower, as can be observed in the current density curves, which leads to better final performance parameters for Zn(sal-3,4-ben) in the PFO:OXD-7 matrix. The fundamental differences of each Zn(II) Schiff base compound were explored in terms of their singlet (S_0 and S_1) and first triplet (T_1) electronic structure calculations under DFT and TD-DFT frameworks. The calculations revealed considerable

View Article Online DOI: 10.1039/D6TC00225F

changes in the Zn(salophen) electronic structure due to the insertion of the benzoyl and benzothiazole moieties, resulting in charge separation between the ground and first excited states at singlet and triplet symmetries, as well, without any influence of the Zn(II) cation in the electronic structures of the molecules. We also correlated all devices' figures of merit with the electrical properties of single-carrier devices, where charge–carrier mobilities, the total density of trap states, and the average energy of traps could be estimated under space-charge conditions during shallow- and deep-trap filling processes, as well as trap-free transport behaviour. In fact, one of the reported critical issues in OLED devices, is the big difference between electrons (usually lower) and holes (higher) electrical mobility, regardless potential barriers at interfaces. Besides that, the different molecular conformation, during (and dependent on) layers deposition, can create a high density of intrinsic defects, that are prone to critically the electrical transport.[44,45] Moreover, the device stability, due to those defects, under an applied electrical field, can leads to a considerable electrical transport change[46,47], with further impacts on the OLEDs figures of merit. In this work, the correlation between molecular systems of the emissive materials and their influence (in simple OLED structure solution-deposited) in the figures of merit, is described, considering the intrinsic defects and their impact on the electrical mobility. With further OLED structure optimized we can achieve an important milestone in the Zn-based first-class organic emitters.

Experimental

Materials

Zn(II) Schiff bases were synthesized previously.[2,3] Poly(ethylenedioxythiophene):poly(4-styrenesulfonate) (PEDOT:PSS) and poly(9,9'-dioctylfluorene) (PFO; M_W = 105.491 g mol^{-1}; PDI = 2.33) polymers, 1,3-bis[2-(4-tert-butylphenyl)-1,3,4-oxadiazo-5-yl]benzene (OXD-7), and etched ITO-glass substrates were purchased from Ossila Company. 2,2',2"-(1,3,5-Benzinetriyl)-tris(1-phenyl-1-H-benzimidazole) (TPBi) was purchased from Lumtech Ltd. Poly(9-vinylcarbazole) (PVK; M_W = 1,100,000 g mol^{-1}), lithium fluoride (LiF; 99.999%), molybdenum(VI) oxide (MoO_3; 99.97%), Hellmanex® and tetrahydrofuran (THF; anhydrous and inhibitor-free grade) were purchased from Sigma–Aldrich, Portugal.

Methods

Electroluminescent devices. Electroluminescent devices were assembled following the standard solution-processable protocol until active-matrix layer deposition, as reported previously[48]. ITO-glass substrates were cleaned under sonication and heat using 2% Hellmanex® solution for 30 minutes. The substrates were subsequently washed with hot water, acetone, and IPA for 15 minutes at each step in a heated ultrasonic bath. Then, the substrates were treated with NaOH (10 vol%) under sonication for 5 minutes, rigorously washed with hot deionized water, and dried with a N_2(g) jet. PEDOT:PSS (30 nm) was dynamically deposited via the spin-coating technique (4000 rpm; 30 s), and the films were annealed in a controlled oven at 120 °C for 10 minutes. Then, the PEDOT:PSS-deposited films were transferred to a N_2(g) controlled atmosphere MBraun Glovebox ([O_2] < 10 ppm; [H_2O] < 0.1 ppm), where a THF solution of PVK (2.591x10^{-2} mol L^{-1}; 5.0 mg mL^{-1}; ≈ 80 nm) was spin-coated, and the active layer containing the Zn(II)salicylidenes (1% mol/mol; eq ≈ 0.05%wt) in PFO and PFO:OXD-7 (THF solution; 2.591x10^{-2} mol L^{-1}; 10.0 mg mL^{-1}) host matrix was subsequently deposited at the same PVK conditions (2000 rpm; 2000 rpm s^{-1}; 60 s). Two set of samples were obtained: 1) without and 2) with thermal annealing at 80 °C for 10 min. Finally, TPBi (30 nm; ETL), LiF (0.5 nm; EIL) and Al (80 nm) electrical contacts were thermally evaporated under ultravacuum conditions (p < 5x10^{-6} mbar), resulting in OLEDs with the following configuration: ITO|PEDOT:PSS|PVK|Active Matrix|TPBi|LiF|Al.

Single-carrier devices. P- and n-type diodes were assembled with the following architecture: ITO|MoO_3|Active layer|MoO_3|Al and ITO|LiF|Active layer|LiF|Al for only hole and electron transport, respectively. MoO_3 (5 nm) thin layers were thermally evaporated at same conditions of LiF and Al, and JxV measurements were the same as those for the full electroluminescent diodes.

OLEDs Optoelectronic characterization. The current and luminance versus voltage curves (J-LxV) of the electroluminescent diodes were measured via a Keithley 2425 source meter coupled with a Konica Minolta CS110 luminancimiter coupled to a close-up lens No. 110, ø=40.5 mm, 20--30 cm, in an Ossila OLED sample holder. EL spectra were acquired via a USB4000 Ocean Optics diode array spectrometer. Luminance and EL measurements were obtained from the normal angle concerning the samples. All OLED figures of merit (current efficiency – η_C, power efficiency – η_P, and external quantum efficiency – EQE) were calculated from homemade software, considering Lambertian emission from devices.

Computational Details. The electronic structure calculations were performed via DFT and its time-dependent counterpart (TDDFT). First, the equilibrium geometries of the metal complexes at their singlet ground states (S_0) were optimized with the CAM-B3LYP exchange-correlation (XC) functional[49] combined with the 6-311++G(d,p) basis set,[50–55] whereas the TD-CAM-B3LYP/6-311++G(d,p) level of theory was used to obtain the equilibrium structures in the first singlet excited state (S_1). Thus, vertical values of absorption and emission energies were obtained considering singlet and/or triplet excited states with the LC-QTP XC functional,[56] combined with the 6-311++G(d,p) basis set. LC-QTP proved to be one of the best XC functionals for describing vertical excitation energies of small molecules[57] as well as of metal complexes.[58] In addition, the natural transition orbitals (NTOs)[59] were also obtained at the LC-QTP/6-311++G(d,p) level. The solvent effects were included via the Polarizable Continuum Method (PCM)[60] Corrected Linear-Response,[61] using the PFO refractive index *n* =1.725 and vacuum permittivity ε = 3. All calculations were carried out within the Gaussian 09 package[62].

Results and discussion

View Article Online
DOI: 10.1039/D5TC03425E

In this work, we adopted two successful strategies for enhancing the optoelectronic properties of asymmetric Zn(salophen)-like coordination compounds into PFO-based (**Fig. 1a**) active-matrix electroluminescent diodes: 1) introducing an electron transport/hole blocking layer (ETL/HBL) to obtain a better electrical balance of injected charge carriers and 2) adding an n-type material inside PFO films to achieve better electron transport in this p-type semiconducting polymer. For this purpose, TPBi and OXD-7 were chosen as ETL/HBL and n-type dopants, respectively. These materials have been widely used in OLEDs for these purposes, and we chose them owing to several specific considerations: TPBi is a good ETM (with an electron mobility of μ_e = 8.0x10^{-5} cm^2 V^{-1} s^{-1})[63] that perfectly matches the energy levels of the highest and lowest occupied molecular orbitals (HOMO and LUMO) of the devices' components (Figures 1b and 1c). In addition, to exhibit the possibility of being an HBL at the same time, combined with the high-molecular-weight PVK HTL property (μ_h = 1.7x10^{-7} cm^2 V^{-1} s^{-1})[64] and EBL (E_{LUMO} = -1.2 eV), our devices are well balanced electrically; OXD-7, in addition to being an excellent ETM (μ_e = 4.0x10^{-5} cm^2 V^{-1} s^{-1})[65], is able to enhance the active-matrix electron transport characteristics. Also, its frontiers orbitals and triplet energy levels combined with PFO energy levels must create a long-lived exciplex state that can be easily transferred to the Zn(II) compounds (Figure 2c). These particular details lead their OLEDs to both better charge-carrier transport and transfer from the host to the guest in the active layers, as discussed below.

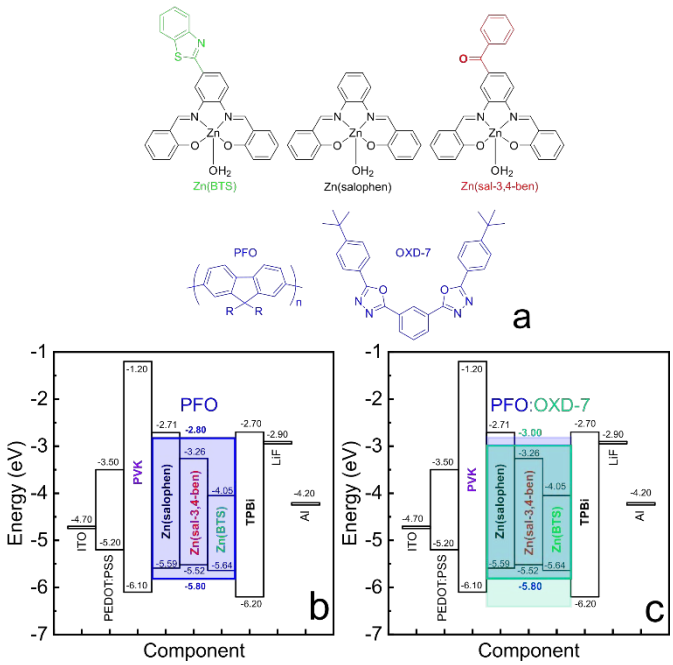

Fig. 1 Molecular structures of the Zn(II) Schiff Base compounds (Zn(BTS), Zn(salophen), and Zn(sal-3,4-ben)) and the host matrices (PFO and OXD-7) (a); energy level diagrams relative to the vacuum level for OLED components using PFO (b) and PFO:OXD-7 (3:2) (c) as hosts matrices.

DFT and TD-DFT calculations were employed to rationalize the distinct optoelectronic behaviours of the Zn(II) Schiff base coordination compounds by examining their singlet and triplet excited-states. The calculated vertical excitation energies for the lowest singlet states reveal that ligand functionalization induces pronounced changes in the low-energy optical transitions (**Table 1**). Zn(salophen) and Zn(BTS) present their first singlet electronic transitions in a similar spectral region (≈ 3.1 and 3.3 eV, respectively), whereas Zn(sal-3,4-ben) exhibits a substantially lower-energy excitation at 2.72 eV. This red-shift originates from the benzoyl substituent, which extends π-conjugation and stabilizes the LUMO level, resulting in a reduced HOMO-LUMO gap relative to the parent salophen structure.

Table 1. Vertical energy values for the first two absorptions ($E_{abs\text{-}vert}$) and the first emission ($E_{emi\text{-}vert}$) transitions with respect to singlet states of the Zn(II) Schiff base compounds, as calculated at the LC-QTP/6-311++G(d,p) level of theory[a].

	$E_{abs\text{-}vert}$ (eV)	$E_{emi\text{-}vert}$ (eV)
Zn(salophen)	3.34 (*f* =0.254)	3.05 (*f*= 0.447)
	3.56 (*f* =0.71)	
Zn(sal-3,4-ben)	2.72 (*f* =0.691)	2.85 (*f* =0.603)
	3.34 (*f* =0.684)	
Zn(BTS)	3.12 (*f* =0.689)	2.86 (*f* =0.901)
	3.39 (*f* =0.989)	

[a] The letter *f* refers to the oscillator strength values.

Despite these differences in vertical excitation, the calculated singlet emission energies show that Zn(BTS) and Zn(sal-3,4-ben) converge toward comparable emissive states (≈ 2.85 and 2.86 eV, respectively), while Zn(salophen) remains blue-shifted (3.05 eV). This behaviour indicates that structural relaxation in the excited state partially compensates for the different electronic gaps present at the ground-state geometry. The relatively large oscillator strengths associated with the emissive singlet transitions confirm that radiative decay from S_1 remains the dominant recombination pathway, consistent with the first-class fluorescent nature of these materials.

Analysis of the triplet-state vertical transitions ($S_0 \rightarrow T_n$) reveal the presence of several low-lying triplet states energetically close to the emissive singlet states for all compounds (**Table 2**). In particular, Zn(salophen) and Zn(sal-3,4-ben) exhibit T_3 states within ~ 0.1 eV of the corresponding singlet emission energies, whereas Zn(BTS) shows a larger separation between these states. Such energetic proximity increases the probability of singlet-triplet interactions under electrical excitation, facilitating exciton trapping and non-radiative recombination processes. The comparatively larger singlet–triplet separation observed for Zn(BTS) suggests a reduced contribution of triplet-mediated quenching pathways, which is expected to be beneficial for electroluminescent performance under high current densities.

Table 2. Vertical energy values (in eV) for the first six triplet-states absorptions of the Zn(II) Schiff base compounds calculated at the LC-QTP/6-311++G(d,p) level of theory, considering PFO as solvent media.

Triplet state	Zn(salophen)	Zn(sal-3,4-ben)	Zn(BTS)
1	2.25	2.18	1.94
2	2.55	2.52	2.46
3	3.07	2.93	2.65
4	3.14	3.01	2.99
5	3.25	3.11	3.05
6	3.95	3.18	3.20

View Article Online
DOI: 10.1039/D5TC04215C

Natural transition orbital (NTO) analysis of the lowest triplet excited state provides further insight into the electronic character of the excited states (**Fig. 2**). Zn(salophen) exhibits a more symmetrical excitation pattern, with hole and electron densities confined to the salophen ligand backbone and minimal spatial separation. In contrast, Zn(sal-3,4-ben) and Zn(BTS) display a marked redistribution of charge density upon excitation, with partial spatial separation of hole- and electron-like NTOs across the ligand framework. The benzoyl and benzothiazole moieties act as electron-accepting fragments, promoting intraligand charge redistribution and giving rise to a quasi-charge-transfer excited state. In all cases, the Zn(II) centre does not contribute directly to the frontier orbitals, confirming its structural role in rigidifying the ligand framework rather than participating in metal-centred electronic transitions, as previous reported[33].

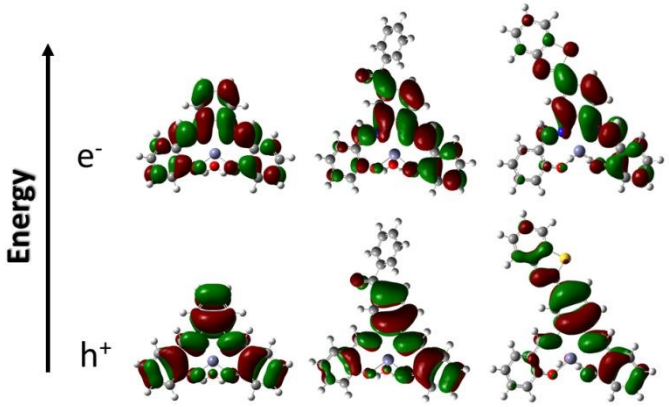

Fig. 2 NTOs associated with the lowest triplet excitation in the Zn(salophen), Zn(sal-3,4-ben), and Zn(BTS) coordination compounds, obtained from LC-QTP/6-311++G(d,p) calculations.

The electroluminescence spectra of the two sets of PFO-based OLEDs are displayed in **Fig. 3** (the insert contain their respective CIE 1931 colour diagram), and **Table 3** summarizes all the OLED figures of merit. PFO and PFO:OXD-7 diodes present quite similar EL behaviour, with zero-phonon (0-0), 0-1, and 0-2 vibronic bands centred at 437, 462, and 500 nm, respectively. A minimal contribution of emission due to aggregated species was observed at ~526 nm. No evidence of OXD-7 EL emission bands could be observed for these devices (λ_{PL} = 347 nm in a THF solution) as a result of complete charge–carrier transfer. The distribution of these EL bands with their intensity confers to PFO and PFO:OXD-7 OLEDs a blue emission colour with chromaticity coordinates at (0.22, 0.25) and (0.23, 0.25), respectively. These EL bands are redshifted compared with those in the studies previously published by our group[38], where the amorphous α-phase of PFO was prevalent. This behaviour is due to differences in the polydispersity index (PDI), molecular weight of the PFO polymer, and polymer chain termination, which are direct consequences of the material supplier. In the present case, electroluminescence of the crystalline β-phase is dominant, which can result in better figures of merit because the active matrix has better crystallinity and, consequently, better charge-transport features[66].

On the other hand, the EL spectra of the polyfluorene derivative with each Zn(II) coordination compound exhibit a combination of both PFO and Zn(II) Schiff's base emission bands (**Fig. 3a** and **3b**). This feature leads to an EL colour close to the white region of the CIE1931 chromaticity diagram (insets of **Fig. 3a** and **3b**), as Zn(II)salophen derivatives present a broad EL band among the green and orange parts of the electromagnetic spectrum (see detailed emission wavelengths in **Table 3**), which, combined with the blue emission colour of the PFO semiconducting polymer, can produce near-white light, according to CIE 1931 chromaticity scale. The addition of the coordination compounds did not considerably disturb the EL bands of the polyfluorene. Changes in the energy and relative intensity of the electroluminescence bands of the polyfluorene derivatives are directly linked to morphological and crystallization behaviour changes. This means that the amount of Zn(salophen), Zn(sal-3,4-ben), and Zn(BTS) added (0.05 wt%) to the PFO and PFO:OXD-7 host matrices is sufficient to observe their EL emission bands because of the energy and charge–carrier transfer from the host to the guests. Therefore, amounts small enough not to yield significant modifications in the morphology of the active layer is desirable for solution-processable OLED and WOLED applications.

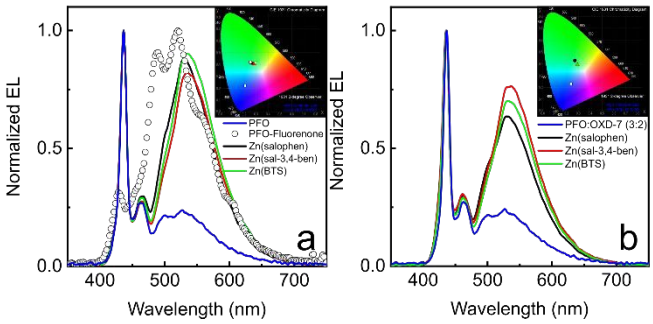

Fig. 3 EL spectra of Zn(II)salicylidene OLEDs in PFO (a) and PFO:OXD-7 (b) host matrices. Insets their respective 2D (x, y) chromaticity colour diagram according to the CIE 1931: blue open squares are PFO and PFO:OXD-7; black open circles are PFO-fluorenone; black circles, red triangles, and green nabla symbols represent the Zn(salophen), Zn(sal-3,4-ben) and Zn(BTS) devices, respectively.

The optoelectronic properties of the PFO- and PFO:OXD-7-based OLEDs were evaluated in terms of current density and brightness versus voltage curves (**Figures 4a** and **4b**, respectively), as were the complete aspects of their figures of merit (EQEs, current and power efficiencies (η_C and η_P, respectively) versus brightness curves (Figure 5c and 5d, respectively). **Table 3** summarizes the global device figures of merit. The devices did not exhibit considerable variation in their turn-on voltages (V_{on}), with values between 4.5 V and 7.0 V (for the PFO:OXD-7 OLED). PFO-based devices exhibit higher brightness (L) values than those assembled with PFO:OXD-7. This behaviour is likely due to the better charge–carrier balance and transport of the modified active layer with the n-type co-host molecule OXD-7. These findings can be clearly observed in the case of the control OLEDs, where the PFO:OXD-7 device presents better figures of merit than the neat PFO OLED: PFO:OXD7 – V_{on} = 7.0 V @ L_{max} = 245 cd m^{-2} @ EQE_{max} = 3.74% @ η_C = 3.38 cd A^{-1} @ η_P = 1.01 lm W^{-1}; PFO – V_{on} = 5.0 V @ L_{max} = 296 cd m^{-2} @ EQE_{max} = 1.59% @ η_C = 1.60 cd A^{-1} @ η_P = 0.83 lm W^{-1} (**Fig. S1**; ESI†).

Table 3. All efficiency parameters of the Zn(II) Schiff-base PFO-based solution-processed OLEDs.

View Article Online
DOI: 10.1039/D6TC00213G

PFO:X	V_{on} (V)	λ_{EL} (nm)	L_{max} (cd m^{-2})	EQE (%)	EQE (100 cd m^{-2})	EQE (1000 cd m^{-2})	η_C (cd A^{-1})	η_P (lm W^{-1})	CIE 1931 (x,y)
PFO (neat)	5.0	437	296	1.59	0.65	-	1.60	0.83	0.22, 0.25
Zn(salophen)	5.0	436; 527	2390	3.18	2.12	0.87	5.16	2.32	0.28, 0.42
Zn(sal-3,4-ben)	4.5	436; 535	3780	2.77	2.09	1.01	4.32	1.94	0.29, 0.42
Zn(BTS)	4.5	437; 534	1850	6.16	1.36	0.56	10.48	5.99	0.30, 0.43
OXD-7	7.0	437	245	3.74	1.99	-	3.38	1.01	0.23, 0.25
OXD-7:Zn(salophen)	4.5	436; 528	1370	2.27	1.55	0.82	3.18	1.54	0.26, 0.43
OXD-7:Zn(sal-3,4-ben)	5.5	435; 536	1770	6.34	1.34	0.75	9.06	4.07	0.28, 0.40
OXD-7:Zn(BTS)	4.5	436; 533	912	3.58	2.08	0.75	4.01	1.80	0.28, 0.40

PFO:OXD-7 (3:2 wt); 0.05%wt of each Zn(II) coordination compound.

When Zn(II) Schiff bases were added to the PFO matrix, we observed an enhancement in the OLED figures of merit in contrast to those of the neat PFO device, as well as those of our previous report, where we did not introduce an electron transport layer on the devices. In this series of OLEDs, better performance features were observed for the PFO:Zn(BTS) device (V_{on} = 4.5 V @ L_{max} = 1850 cd m^{-2} @ EQE_{max} = 6.16% @ η_C = 10.48 cd A^{-1} @ η_P = 5.99 lm W^{-1}). Although Zn(salophen)- and Zn(sal-3,4-ben)-based devices have lower figures of merit, they have shown high brightness values (L_{max} = 2390 and 3780 cd m^{-2}, respectively) coupled with lower OLED roll-off (R_{off}) losses than Zn(BTS)-based devices: Zn(BTS) – EQE(100 cd m^{-2}) = 1.36% @ R_{off} = 78%, EQE(1000 cd m^{-2}) = 0.56% @ R_{off} = 91%; Zn(sal-3,4-ben) – EQE(100 cd m^{-2}) = 2.09% @ R_{off} = 24%, EQE(1000 cd m^{-2}) = 1.01% @ R_{off} = 63%; and Zn(Salophen) – EQE(100 cd m^{-2}) = 2.12% @ R_{off} = 33%, EQE(1000 cd m^{-2}) = 0.87% @ R_{off} = 73%.

In contrast, when the n-type co-host (OXD-7) was added to the active layer to improve the charge–carrier transport and balance, better figures of merit can be observed for the Zn(sal-3,4-ben)-based OLED (V_{on} = 5.0 V @ L_{max} = 1770 cd m^{-2} @ EQE_{max} = 6.34% @ η_C = 9.06 cd A^{-1} @ η_P = 4.07 lm W^{-1}). The R_{off} values are the same as those observed for PFO-based devices, i.e., better maxima reflect high-efficiency losses with increasing brightness values: Zn(BTS) – EQE(100 cd m^{-2}) = 2.08% @ R_{off} = 42%, EQE(1000 cd m^{-2}) = 0.75% @ R_{off} = 79%, Zn(sal-3,4-ben) – EQE(100 cd m^{-2}) = 1.34% @ R_{off} = 79%, EQE(1000 cd m^{-2}) = 1.01% @ R_{off} = 88%, and Zn(salophen) – EQE(100 cd m^{-2}) = 1.55% @ R_{off} = 32%, EQE(1000 cd m^{-2}) = 0.82% @ R_{off} = 64%.

Importantly, Zn(salophen)-based OLEDs, although presenting lower figures of merit on the PFO:OXD-7 matrix, exhibit similar roll-off values in both types of devices, whereas Zn(BTS) and Zn(sal-3,4-ben) compounds have better performance on PFO and PFO:OXD-7 OLEDs, respectively. This behaviour can be closely related to the electronic structure dipole orientation and molecular orbital orientation in both types of devices, as Zn(BTS) and Zn(sal-3,4-ben) present a quasi-charge transfer electronic state. Therefore, the Zn(salophen) coordination compound is expected to be less susceptible to chemical environment effects, as reflected in its OLED R_{off} behaviour. On the other hand, adding benzophenone and benzothiazole moieties increases the susceptibility of the optoelectronic properties of Zn(II)Schiff-based coordination compounds to media into thin films: a partial overview of the observed behaviour of PFO- and PFO:OXD-7-based OLEDs, due to their quasi-charge-transfer behaviour.

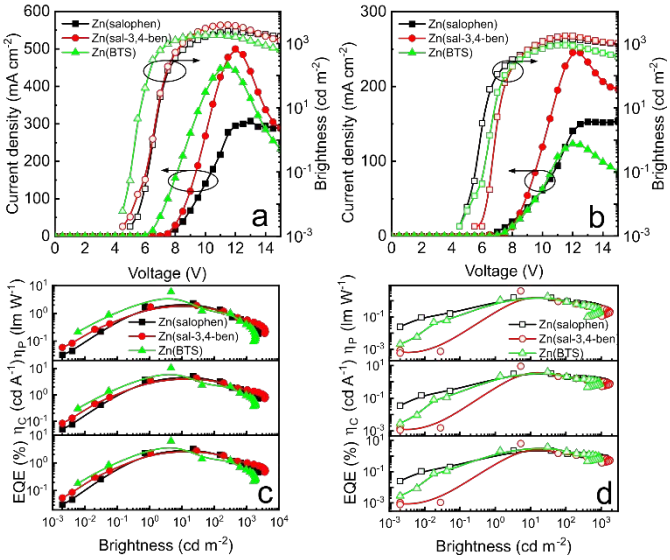

Fig. 4 Current density (full symbols) and brightness (open symbols) versus voltage and operational figures of merit (EQE, η_C and η_P) versus brightness curves of the Zn(II) Schiff-based OLEDs in the PFO (a and c) and PFO:OXD-7 (b and d) matrices.

To better understand the optoelectronic features observed in both series of solution-processed OLEDs, we successfully employed space-charge limited-current models for electron- and hole-only devices, as Mott–Gurney's law describes,[67] following equation 1:

$$J_{SCLC} = \frac{9}{8}\varepsilon\varepsilon_0\mu_i\frac{V^2}{L^3} \qquad \textbf{(Equation 1)}$$

where J_{SCLC} is the current density in the SCLC domain, e is the active layer dielectric constant (~ 3 for most semiconducting organic materials), e_0 is the free-space electrical permittivity, μ_i is the charge carrier mobility (i = e for electron-only devices; and i = h for hole-only devices) in the SCLC region, V is the applied bias, and L is the active layer thickness. **Table 4** summarizes the electrical properties of OLEDs and only type devices.

The μ_i values were calculated during the shallow-trap filling processes, where JxV curves (**Fig. S2** to **S5**; **Tables S4** to **S7**; ESI†) respect the quadratic law (J α V^2)[68], and we can easily observe how each coordination compound, as well as the OXD-7 co-host, impact the trap-filling behaviour of the devices. As a general rule, the addition of the OXD-7 co-host into the PFO matrix causes devices to have a

View Article Online
DOI: 10.1039/D6TC00213G

Table 4. Electric characteristics of Zn(II) Schiff base PFO-based solution-processed OLEDs.

PFO:X	V_{TFL} (V)	N_T (cm^{-3})	E_T (meV)	$\mu_{TF^{SCLC}}$ ($cm^2\ V^{-1}\ s^{-1}$)	μ_h ($cm^2\ V^{-1}\ s^{-1}$)	μ_e ($cm^2\ V^{-1}\ s^{-1}$)
PFO (neat)	4.75	$2.46x10^{17}$	399	$3.38x10^{-8}$	$3.70x10^{-10}$	$3.27x10^{-11}$
Zn(salophen)	6.26	$3.24x10^{17}$	673	$1.01x10^{-7}$	$3.65x10^{-10}$	$1.95x10^{-11}$
Zn(sal-3,4-ben)	6.07	$3.14x10^{17}$	701	$1.81x10^{-7}$	$3.44x10^{-10}$	$6.78x10^{-12}$
Zn(BTS)	4.96	$2.57x10^{17}$	738	$1.95x10^{-7}$	$1.26x10^{-9}$	$1.48x10^{-10}$
OXD-7	9.00	$4.66x10^{17}$	662	$2.03x10^{-9}$	$8.00x10^{-10}$	$2.23x10^{-12}$
OXD-7:Zn(salophen)	5.12	$2.65x10^{17}$	522	$4.79x10^{-8}$	$3.17x10^{-10}$	$3.19x10^{-12}$
OXD-7:Zn(sal-3,4-ben)	3.38	$1.75x10^{17}$	191	$8.55x10^{-8}$	$9.04x10^{-7}$	$4.91x10^{-12}$
OXD-7:Zn(BTS)	3.50	$1.81x10^{17}$	218	$4.44x10^{-8}$	$3.11x10^{-10}$	$5.42x10^{-12}$

PFO:OXD-7 (3:2 wt); 0.05%wt of each Zn(II) coordination compounds.

poor electrical balance between the injected electrons and holes in the active layer, with a ratio between μ_e and μ_h ($\frac{\mu_e}{\mu_h}$), in the case of PFO-based devices, just one order of magnitude (10^{-1}) lower, and for PFO:OXD-7, at least two orders of magnitude (10^{-2}) lower. The differences in the charge–carrier transport balance between the PFO and PFO:OXD-7 devices can be directly attributed to the fact that OXD-7-based OLEDs exhibit lower brightness values than PFO devices. Additionally, higher roll-off losses have been reported for the devices that possess large charge–carrier disbalances, as to the case of PFO:OXD-7:Zn (sal-3,4-ben) OLEDs. Although this device presents the highest EQE values in contrast to the others, which have higher roll-off rates. At the same time, PFO:OXD-7:Zn (sal-3,4-ben) device possess a $\frac{\mu_e}{\mu_h}$ ratio five orders of magnitude lower of electrical balance ($\frac{\mu_e}{\mu_h} \approx 10^{-5}$). Additionally, we estimated the electrical mobility (μ_{SCLC}^{TF}) in the trap-free region (Child's law)[68] of the OLEDs' JxV curves and found more conclusive correlations between the OLEDs' performance and the electronic mobility of the minority charge carrier, in our case, electrons. In Child's domain, devices with better electron mobility led to high-performance OLEDs, such as PFO- and PFO:OXD-7-based devices Zn(BTS) and Zn(sal-3,4-ben), respectively (see detailed values in **Tables 3** and **4**).

In addition, we determine the total density of trap states (N_T) at the point where Mott–Gurney's law meets Mark–Helfrich's deep-trap filling relationship, also known as the trap-filled voltage (V_{TFL})[69], which follows equation 2:

$$V_{TFL} = \frac{qN_TL^2}{2\varepsilon\varepsilon_0} \qquad \textbf{(Equation 2)}$$

where q is the elementary charge. Also, from the slope m of the JxV data in logarithmic scale, we can extract the trap energy from the Fermi level as $m = T_t/T$, being T_t the characteristic trap temperature (which will give the correspondent energy) and T the temperature.[14]

In the first case (PFO OLEDs), the insertion of Zn(II)Schiff bases on the active matrix enhances the density of trap states. In contrast, the very low amount of Zn(II) coordination compounds added to PFO:OXD-7 mixture diminishes the N_T. The neat PFO device presented lower N_T than PFO:OXD-7 OLED. Besides, the addition of Zn (salicylidenes) into the PFO:OXD-7 matrix leads to lower N_T values than those of PFO devices (see **Table 4**). It is worth mentioning that devices with a lower density of trap states and average trap energy (E_T) present high figures of merit, as expected for most OLEDs.

The electroluminescent performance achieved in this work represents a substantial advance relative to previously reported Zn(II) Schiff base based OLEDs. In earlier studies by Germino et al.[37], devices employing PVK as the host matrix and lacking dedicated electron-transport engineering exhibited external quantum efficiencies below 0.5%, primarily due to limited charge-carrier mobility, low photoluminescence quantum yield of the emissive layer, and insufficient energetic overlap between host and guest materials. Subsequent work by Duarte et al.[38] demonstrated that replacing PVK with PFO led to enhanced electroluminescence intensity and improved spectral overlap with the absorption of the Zn(II) complexes, owing to the higher hole mobility and photoluminescence efficiency of PFO. Nevertheless, in the absence of an electron-transport layer, the best-performing devices remained constrained by trap-assisted recombination and pronounced charge imbalance, yielding EQE values limited to approximately 0.52%.

In the present work, although the devices exhibit comparable turn-on voltages (V_{on} = 4.5 ~ 7.0 V), their luminance and efficiency behaviour differ significantly depending on the host matrix. PFO-based devices reach higher maximum luminance values (up to 3780 cd m^{-2} for Zn(sal-3,4-ben)), which reflects larger injected current densities. However, SCLC analysis (**Table 4**) reveals that incorporation of Zn(II) Schiff bases into PFO increases the trap-state density ($N_T \approx 3.1$ ~ $3.2x10^{17}$ cm^{-3}) and is associated with relatively deep trap energies (E_T = 673 ~ 738 meV), which favour trap-assisted recombination and efficiency losses at higher current densities.

In contrast, when OXD-7 is incorporated as an n-type co-host, the electrical behaviour changes substantially. For the optimized PFO:OXD-7:Zn(sal-3,4-ben) device, the trap-state density decreases to $1.75x10^{17}$ cm^{-3} and the average trap energy is reduced to 191 meV. Additionally, the trap-filled limit voltage decreases to 3.38 V, indicating earlier trap filling and a more efficient transition toward trap-free transport. Although the absolute μ_e values remain lower than μ_h, the reduced trap density and shallower traps mitigate trap-assisted recombination, leading to improved charge recombination efficiency.

Consequently, while PFO-based devices achieve higher luminance, the PFO:OXD-7 matrix provides superior external quantum efficiency (EQE = 6.34%) due to reduced trap-mediated losses and improved carrier recombination efficiency rather than increased current injection. This distinction highlights that luminance

and recombination efficiency are not directly proportional and must be interpreted in conjunction with charge-transport parameters.

Finally, the present study implements two complementary strategies to overcome these limitations: the insertion of TPBi as an electron-transport and hole-blocking layer and the incorporation of OXD-7 as an n-type co-host to form an exciplex-capable PFO-based active matrix. These modifications result in a pronounced enhancement of charge-carrier balance and exciton confinement, enabling devices with external quantum efficiencies exceeding 6%, current efficiencies up to 10.48 cd A^{-1}, and turn-on voltages as low as 4.5-5.0 V. The performance gains are quantitatively supported by SCLC analysis, which reveals reduced trap-state densities (down to ~10^{17} cm^{-3}), lower average trap energies (< 200 meV in optimized systems), and improved minority-carrier (electron) mobilities in the highest-efficiency devices. These electrical characteristics correlate directly with the DFT-derived excited-state properties: Zn(BTS) and Zn(sal-3,4-ben), which exhibit quasi-charge-transfer character and modified singlet-triplet energetic landscapes, show enhanced compatibility with the engineered host environments, resulting in reduced trap filling and more efficient charge recombination. The combined experimental and theoretical analysis thus establishes a clear structure/property/performance relationship, demonstrating that rational ligand design coupled with targeted transport-layer engineering enables first-class Zn(II) fluorescent emitters to approach or slightly surpass the conventional ~5% EQE benchmark commonly associated with first-class fluorescent emitters in standard architectures for near-white OLEDs, while maintaining moderate efficiency roll-off.

Conclusions

This study demonstrates that Zn(II) Schiff base coordination compounds can function as efficient emissive dopants in solution-processed OLEDs when combined with rational host and interface engineering. The incorporation of TPBi as an electron-transport/hole-blocking layer and the use of OXD-7 as an n-type co-host in PFO-based matrices significantly improve charge-carrier balance and exciton confinement, leading to near-white electroluminescence with external quantum efficiencies exceeding 6%, current efficiencies above 10 cd A^{-1}, and reduced turn-on voltages. Electronic structure calculations reveal that ligand functionalization strongly modifies the molecular excited-states, inducing quasi-charge-transfer character in Zn(BTS) and Zn(sal-3,4-ben) while preserving ligand-centred fluorescence. These features govern singlet-triplet energetic proximity and host sensitivity without direct participation of the Zn(II) centre in frontier orbitals. SCLC analysis establishes a direct correlation between molecular design and device performance, showing that high-efficiency devices exhibit reduced trap-state densities, lower average trap energies, and enhanced minority-carrier mobilities. Overall, the results establish a relationship linking coordination chemistry, excited-state electronic structure, and charge-transport dynamics. This work demonstrates that first-class Zn(II) fluorescent emitters can approach or surpass conventional theoretical efficiency limits for near-white OLEDs, providing a viable pathway toward low-cost, solution-processable devices based on Earth-abundant materials.

Author contributions

J. C. G. (Conceptualization: Lead; Investigation: Lead; Methodology: Lead; Funding acquisition: Lead; Writing – original draft: Lead; Writing – review & editing: Lead). R. A. M. (Conceptualization: Supporting; Investigation: Equal; Methodology: Equal; Visualization: Supporting; Theoretical calculations: Lead; Writing – original draft: Supporting; Writing – review & editing: Equal). L G. T. A. D. (Conceptualization: Supporting; Investigation: Supporting; Methodology: Equal; Visualization: Supporting; Writing – original draft: Equal; Writing – review & editing: Equal). F. S. R. (Investigation: Supporting; Resources: Supporting; Writing – original draft: Supporting; Writing – review & editing: Equal). R. L A. H. (Methodology: Supporting; Resources: Supporting). L. P. (Conceptualization: Equal; Funding acquisition: Lead; Investigation: Equal; Methodology: Equal; Resources: Lead; Writing – review & editing: Lead)

Conflicts of interest

There are no conflicts to declare.

Data availability

The data supporting the findings of this study are available in the manuscript and its SI.

Acknowledgements

J.C.G. and L.P. acknowledge the Institute for Nanostructures, Nanomodelling, and Nanofabrication (i3N)-associated laboratory of the Portuguese Foundation for Science and Technology (FCT) (UIDB/50025/2020 & LA/P/0037/2020). J.C.G. also thanks FCT/i3N/UA for the individual CEEC grant (2021.02056.CEECIND). R.L.A.H. and F.S.R. also thank CNPq for financial support (306763/2021-4; 304368/2023-7).

References

1 C. W. Tang and S. A. Vanslyke, *Appl. Phys. Lett.*, 1987, **51**, 913–915.

2 O. Sachnik, N. Kinaret, R. Saxena, M. Manz, W. Liu, J. T. Blaskovits, D. Andrienko, J. J. Michels, P. W. M. Blom and G. J. A. H. Wetzelaer, *Nat. Mater.*, DOI:10.1038/s41563-025-02294-8.

3 X. Wu, S. Ni, C.-H. Wang, W. Zhu and P.-T. Chou, *Chem. Rev.*, 2025, **125**, 6685–6752.

4 L. Yao, Y. Qin, X. Li, Q. Xue, F. Liu, T. Cheng, G. Li, X. Zhang and W. Lai, *InfoMat*, DOI:10.1002/inf2.12410.

5 B. Kulyk, J. C. Germino, D. Gaspar, A. J. S. Fernandes, J. Deuermeier, A. F. Carvalho, A. F. da Cunha, L. M. N. Pereira, L. Pereira and F. M. Costa, *J. Mater. Chem. C Mater.*, 2025, **13**, 5855–5864.

6 J. Eccher, W. Zajaczkowski, G. C. Faria, H. Bock, H. von Seggern, W. Pisula and I. H. Bechtold, *ACS Appl. Mater. Interfaces*, 2015, **7**, 16374–16381.

7 F. M. Xie, Z. D. An, M. Xie, Y. Q. Li, G. H. Zhang, S. J. Zou, L. Chen, J. De Chen, T. Cheng and J. X. Tang, *J. Mater. Chem. C Mater.*, 2020, **8**, 5769–5776.

8 Q. S. Tian, W. S. Shen, Y. J. Yu, X. Q. Wang, J. H. Cai, Y. Hu, Z. Q. Jiang, J. S. Huang and L. S. Liao, *Org. Electron.*, 2022, **100**, 106366.

9 C. Kant, A. Shukla, S. K. M. McGregor, S. C. Lo, E. B. Namdas and M. Katiyar, *Nat. Commun.*, DOI:10.1038/s41467-023-43014-7.

10 A. C, D. K. Dubey, M. Pahlevani and G. C. Welch, *Adv. Mater. Technol.*, DOI:10.1002/admt.202100264.

11 X. Fan, X. Hao, F. Huang, J. Yu, K. Wang and X. Zhang, *Advanced Science*, 2023, **2303504**, 1–24.

12 E. S. Moraes, J. C. Germino and L. Pereira, *Org. Electron.*, DOI:10.1016/j.orgel.2024.107175.

13 G. Hong, X. Gan, C. Leonhardt, Z. Zhang, J. Seibert, J. M. Busch and S. Bräse, *Advanced Materials*, DOI:10.1002/adma.202005630.

14 L. Pereira, *Organic Light Emitting Diodes The Use of Rare Earth and Transition Metals*, Jenny Stanford Publishing; CRC Press: Taylor & Francis Group, Boca Raton, USA, 2012.

15 T. Scharff, W. Ratzke, J. Zipfel, P. Klemm, S. Bange and J. M. Lupton, *Nat. Commun.*, 2021, **12**, 2071.

16 N. Ledos, D. Tondelier, B. Geffroy, D. Jacquemin, P.-A. Bouit and M. Hissler, *J. Mater. Chem. C Mater.*, 2023, **11**, 3826–3831.

17 C. Wu, M. Wang, K. Tong, M. Zhang, W. Li, Z. Xu, W. Zhang, Y. Wu, C. Yang, H. Fu, S. S. Chen, M. Ng, M. Tang and G. Wei, *Adv. Opt. Mater.*, DOI:10.1002/adom.202201998.

18 M.-C. Tang, M.-Y. Chan and V. W.-W. Yam, *Chem. Rev.*, 2021, **121**, 7249–7279.

19 S. K. Mizoguchi, G. Santos, A. M. Andrade, F. J. Fonseca, L. Pereira and N. Y. Murakami Iha, *Synth. Met.*, 2011, **161**, 1972–1975.

20 B.-S. S. Du, J.-L. L. Liao, M.-H. H. Huang, C.-H. H. Lin, H.-W. W. Lin, Y. Chi, H.-A. A. Pan, G.-L. L. Fan, K.-T. T. Wong, G.-H. H. Lee and P.-T. T. Chou, *Adv. Funct. Mater.*, 2012, **22**, 3491–3499.

21 J. C. Germino, L. G. T. A. Duarte, R. A. Mendes, M. M. Faleiros, A. de Morais, J. N. de Freitas, L. Pereira and T. D. Z. Atvars, *Nanomaterials*, 2022, **12**, 2497.

22 P. L. dos Santos, P. Stachelek, Y. Takeda and P. Pander, *Mater. Chem. Front.*, 2024, **8**, 1731–1766.

23 E. Tankelevičiūtė, I. D. W. Samuel and E. Zysman-Colman, *J. Phys. Chem. Lett.*, 2024, **15**, 1034–1047.

24 J. M. Dos Santos, D. Hall, B. Basumatary, M. Bryden, D. Chen, P. Choudhary, T. Comerford, E. Crovini, A. Danos, J. De, S. Diesing, M. Fatahi, M. Griffin, A. K. Gupta, H. Hafeez, L. Hämmerling, E. Hanover, J. Haug, T. Heil, D. Karthik, S. Kumar, O. Lee, H. Li, F. Lucas, C. F. R. Mackenzie, A. Mariko, T. Matulaitis, F. Millward, Y. Olivier, Q. Qi, I. D. W. Samuel, N. Sharma, C. Si, L. Spierling, P. Sudhakar, D. Sun, E. Tankelevičiūtė, M. Duarte Tonet, J. Wang, T. Wang, S. Wu, Y. Xu, L. Zhang and E. Zysman-Colman, *Chem. Rev.*, 2024, **124**, 13736–14110.

25 X. Zhang, J. Song, X. Chang, K. Li and Y. Chen, *Chemistry – A European Journal*, DOI:10.1002/chem.202304224.

26 M. J. Leitl, D. M. Zink, A. Schinabeck, T. Baumann, D. Volz and H. Yersin, *Top. Curr. Chem.*, 2016, **374**, 25.

27 M. Yu. Petyuk, L. Meng, Z. Ma, A. M. Agafontsev, I. Yu. Bagryanskaya, A. S. Berezin, J. Zhang, A. Chu, M. I. Rakhmanova, H. Meng, A. V. Tkachev, V. W. Yam and A. V. Artem'ev, *Angewandte Chemie International Edition*, DOI:10.1002/anie.202412437.

28 J.-G. Yang, N. Li, J. Li, X.-F. Song, M.-D. Li, J. Zhang and K. Li, *J. Mater. Chem. A Mater.*, 2024, **12**, 18977–18985.

29 P. Pander, Y. M. Dikova, E. V. Puttock and J. A. G. Williams, *Inorg. Chem. Front.*, 2024, **11**, 7545–7551.

30 J.-G. Yang, X. Feng, N. Li, J. Li, X.-F. Song, M.-D. Li, G. Cui, J. Zhang, C. Jiang, C. Yang and K. Li, *Sci. Adv.*, DOI:10.1126/sciadv.adh0198.

31 P. K. Petrova, R. L. Tomova, R. T. Stoycheva-Topalova, S. S. Kaloyanova and T. G. Deligeorgiev, *J. Lumin.*, 2012, **132**, 495–501.

32 K. Singh, I. Siddiqui, V. Sridharan, R. A. Kumar Yadav, J.-H. Jou and D. Adhikari, *Inorg. Chem.*, 2021, **60**, 19128–19135.

33 M. G. Vivas, J. C. Germino, C. A. Barboza, P. A. M. Vazquez, L. De Boni, T. D. Z. Atvars and C. R. Mendonça, *Journal of Physical Chemistry C*, 2016, **120**, 4032–4039.

34 S. Frassinetti, G. L. Bronzetti, L. Caltavuturo, M. Cini and C. Della Croce, *Journal of Environmental Pathology, Toxicology and Oncology*, 2006, **25**, 597–610.

35 E. S. Moraes, L. G. T. A. Duarte, F. S. Rodembusch, J. C. Germino, L. F. R. Pereira and T. D. Z. Atvars, *Mater. Adv.*, 2024, **5**, 7778–7788.

36 K. Khanmohammadi Chenab, F. Zarifi, M. R. Zamani Meymian and S. Mahmoudi Qashqay, *Nanoscale Adv.*, DOI:10.1039/D5NA00450K.

37 J. C. Germino, J. N. de Freitas, R. A. Domingues, F. J. Quites, M. M. Faleiros and T. D. Z. Atvars, *Synth. Met.*, 2018, **241**, 7–16.

38 L. G. T. A. Duarte, J. C. Germino, R. A. Mendes, J. F. Berbigier, K. S. Moreira, M. M. Faleiros, J. N. de Freitas, T. A. L. Burgo, F. S. Rodembusch and T. D. Z. Atvars, *The Journal of Physical Chemistry C*, 2020, **124**, 21036–21046.

39 Y. Shi, M. Sun, H. Shi, Z. Liang, B. Qiao, S. Zhao, X. Pu and D. Song, *Sci. Bull. (Beijing).*, DOI:10.1016/j.scib.2025.07.007.

40 X. Lu, Q. Wang, X. Cai, Y. Qu, Z. Li, C. Li and Y. Wang, *Adv. Funct. Mater.*, DOI:10.1002/adfm.202313897.

41 S.-C. Lo, N. A. H. Male, J. P. J. Markham, S. W. Magennis, P. L. Burn, O. V. Salata and I. D. W. Samuel, *Advanced Materials*, 2002, **14**, 975–979.

42 Z. Gao, C. S. Lee, I. Bello, S. T. Lee, R.-M. Chen, T.-Y. Luh, J. Shi and C. W. Tang, *Appl. Phys. Lett.*, 1999, **74**, 865–867.

43 C.-C. Yang, C.-J. Hsu, P.-T. Chou, H. C. Cheng, Y. O. Su and M. Leung, *J. Phys. Chem. B*, 2010, **114**, 756–768.

44 V. M. Silva and L. Pereira, *J. Non. Cryst. Solids*, 2006, **352**, 5429–5436.

45 K. Yang, S. Nam, J. Kim, J. W. Kim and J. Lee, *Adv. Opt. Mater.*, DOI:10.1002/adom.202301853.

46 V. M. Silva, S. K. Mendiratta and L. Pereira, *J. Non. Cryst. Solids*, 2006, **352**, 1652–1655.

47 L. Chen, S. Wang, K. Zhang, A. Wang, Y. Fang and Z. Du, *Org. Electron.*, 2019, **66**, 110–115.

48 F. Teixeira, J. C. Germino and L. Pereira, *Applied Sciences*, 2023, **13**, 12020.

49 T. Yanai, D. P. Tew and N. C. Handy, *Chem. Phys. Lett.*, 2004, **393**, 51–57.

50 R. Ditchfield, W. J. Hehre and J. A. Pople, *J. Chem. Phys.*, 1971, **54**, 720–723.

51 M. M. Francl, W. J. Pietro, W. J. Hehre, J. S. Binkley, M. S. Gordon, D. J. DeFrees and J. A. Pople, *J. Chem. Phys.*, 1982, **77**, 3654–3665.

52 M. S. Gordon, J. S. Binkley, J. A. Pople, W. J. Pietro and W. J. Hehre, *J. Am. Chem. Soc.*, 1982, **104**, 2797–2803.

53 P. C. Hariharan and J. A. Pople, *The Influence of Polarization Functions on Molecular Orbital Hydrogenation Energies*, Springer-Verlag, 1973, vol. 28.

54 W. J. Hehre, K. Ditchfield and J. A. Pople, *J. Chem. Phys.*, 1972, **56**, 2257–2261.

55 V. A. Rassolov, J. A. Pople, M. A. Ratner and T. L. Windus, *Journal of Chemical Physics*, 1998, **109**, 1223–1229.

56 R. L. A. Haiduke and R. J. Bartlett, *Journal of Chemical Physics*, DOI:10.1063/1.5025723.

57 R. A. Mendes, R. L. A. Haiduke and R. J. Bartlett, *J. Chem. Phys.*, DOI:10.1063/5.0035446.

58 R. A. Mendes and R. L. A. Haiduke, *Theor. Chem. Acc.*, DOI:10.1007/s00214-021-02844-8.

59 R. L. Martin, *Journal of Chemical Physics*, 2003, **118**, 4775–4777.

60 S. Miertuš, E. Scrocco and J. Tomasi, *Chem. Phys.*, 1981, **55**, 117–129.

61 M. Caricato, B. Mennucci, J. Tomasi, F. Ingrosso, R. Cammi, S. Corni and G. Scalmani, *J. Chem. Phys.*, DOI:10.1063/1.2183309.

62 Frisch, G. Trucks, H. Schlegel, G. Scuseria, M. Robb, J. Cheeseman, G. Scalmani, V. Barone, B. Mennucci, G. Petersson, H. Nakatsuji, M. Caricato, X. Li, H. Hratchian, A. Izmaylov, J. Bloino, G. Zheng, J. Sonnenberg, M. Hada, M. Ehara, K. Toyota, R. Fukuda, J. Hasegawa, M. Ishida, T. Nakajima, Y. Honda, O. Kitao, H. Nakai, T. Vreven, J. Montgomery, J. Peralta, F. Ogliaro, M. Bearpark, J. Heyd, E. Brothers, K. Kudin, V. Staroverov, R. Kobayashi, J. Normand, K. Raghavachari, A. Rendell, J. Burant, S. Iyengar, J. Tomasi, M. Cossi, N. Rega, J. Millam, M. Klene, J. Knox, J. Cross, V. Bakken, C. Adamo, J. Jaramillo, R. Gomperts, R. Stratmann, O. Yazyev, A. Austin, R. Cammi, C. Pomelli, J. Ochterski, R. Martin, K. Morokuma, V. Zakrzewski, G. Voth, P. Salvador, J. Dannenberg, S. Dapprich, A. Daniels, Farkas, J. Foresman, J. Ortiz, J. Cioslowski and D. Fox, *Gaussian 09, Revision B.01, Gaussian, Inc., Wallingford CT*.

63 Y. Wang, B. Li, C. Jiang, Y. Fang, P. Bai and Y. Wang, *Journal of Physical Chemistry C*, 2021, **125**, 16753–16758.

64 J. Jeong, J. Lee, H. Lee, G. Hyun, S. Park, Y. Yi, S. W. Cho and H. Lee, *Chem. Phys. Lett.*, 2018, **706**, 317–322.

65 Y.-T. Chang, J.-K. Chang, Y.-T. Lee, P.-S. Wang, J.-L. Wu, C.-C. Hsu, I.-W. Wu, W.-H. Tseng, T.-W. Pi, C.-T. Chen and C.-I. Wu, *ACS Appl. Mater. Interfaces*, 2013, **5**, 10614–10622.

66 M. N. Yu, H. Soleimaninejad, J. Y. Lin, Z. Y. Zuo, B. Liu, Y. F. Bo, L. B. Bai, Y. M. Han, T. A. Smith, M. Xu, X. P. Wu, D. E. Dunstan, R. D. Xia, L. H. Xie, D. D. C. Bradley and W. Huang, *Journal of Physical Chemistry Letters*, 2018, **9**, 364–372.

67 N. F. Mott and R. W. Gurney, *Electronic Processes in Ionic Crystals*, Oxford University Press, London, UK, 2nd edn., 1948.

View Article Online
DOI: 10.1039/D6TC00213G

68 M. Pope and C. E. Swenberg, *Electronic Processes in Organic Crystals and Polymers*, Oxford University Press, 1999.

69 P. Mark and W. Helfrich, *J. Appl. Phys.*, 1962, **33**, 205–215.